ACS Energy LETTERS

http://pubs.acs.org/journal/aelccp

LETTER

Electrochemical Lithiation of Covalently Bonded Sulfur in Vulcanized Polyisoprene

Chengyin Fu,[†] Guanghui Li,[†,‡] Jian Zhang,[†] Benjamin Cornejo,[†] Sophie S. Piao,[§] Krassimir N. Bozhilov,[∥] Robert C. Haddon,[†,‡,⊥] and Juchen Guo*[,†]

[†]Department of Chemical and Environmental Engineering, [‡]Center for Nanoscale Science and Engineering, [∥]Central Facility for Advanced Microscopy and Microanalysis, and [⊥]Department of Chemistry, University of California, Riverside, California 92521, United States

[§]Division of Chemistry and Chemical Engineering, California Institute of Technology, Pasadena, California 91125, United States

Supporting Information

ABSTRACT: We report the synthesis of vulcanized polyisoprene (SPIP) nanowires and an investigation of the electrochemical lithiation mechanism of the covalently bonded sulfur bridges in SPIP. Electrochemical analysis demonstrates that the sulfur chains in SPIP have distinct electrochemical signatures from those that are characteristic of bulk elemental sulfur. The cyclic voltammetry and galvanostatic cycling data show a distinct multistep charge-transfer process and solid-state lithium−sulfur reaction behavior, and it is clear that this new material provides a promising basis for the development of cathodes for rechargeable batteries. Chemical changes due to the lithiation process are studied using Raman and X-ray photoelectron spectroscopy, on the basis of which new lithiation mechanisms of covalently bonded sulfur are proposed.

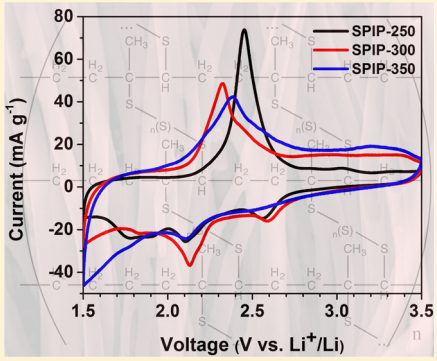

Lithium−sulfur (Li−S) batteries have been considered as a promising alternative energy storage technology to the current lithium ion batteries. Some of the greatest technical challenges faced by Li−S batteries originate from the complex lithiation−delithiation process of sulfur, which goes through solid−liquid−solid multiphase reactions involving numerous intermediate polysulfides. The majority of current sulfur-based cathode materials are composites, which means that the electrochemical reactions start with elemental sulfur. On the other hand, electrochemically active sulfur chains covalently bonded to a carbonaceous matrix may have very different lithiation−delithiation mechanisms from elemental sulfur,[1,2] but high-performance organosulfur compounds of this type have yet to be fully developed. In order to achieve high capacity, covalently bonded sulfur chains are preferable, and one of such a material is derived from a sulfur-polyacrylonitrile (S-PAN) organosulfur polymer.[3−7] The structure of S-PAN can be generally described as short sulfur chains tethered on ribbon-like backbones composed of nitrogen-containing heterocyclic groups.[8] A recent study by Wei and co-workers more specifically suggests that only disulfide and trisulfide chains are tethered in S-PAN, which leads to a solid-state lithiation−delithiation reaction eliminating the formation of lithium polysulfide species.[9] More recently, a different type of polymeric organosulfur cathode material has been synthesized by polymerizing long sulfur chains (as diradicals) with linker monomers having two or three functional groups that are subject to free radical addition reactions including vinyl,[10−13] ethynyl,[14,15] sulfhydryl,[16] and nitrile.[17] Due to their general structure mainly composed of long sulfur chains and short polymeric cross-linkers, the synthetic methodology of these organosulfur compounds is named "inverse vulcanization". A common trait of these organosulfur polymers is that they all have sulfur backbones, and thus, their electrochemical characteristics are similar to bulk sulfur.

On the other hand, vulcanized natural rubber represents an organosulfur polymer with an inverse structure to the inversely vulcanized organosulfur polymers as it is composed of a polyisoprene (PIP) backbone cross-linked by sulfur chains. We reasoned that the bridging sulfur chains (S_n with $n \geq 2$) should be electrochemically active and might have unique characteristics due to the tight chemical and physical bonding to the PIP matrix. Vulcanized PIP (denoted as SPIP) is composed of carbon−carbon single bonds, carbon−carbon double bonds, and carbon−sulfur single bonds, as illustrated in Scheme 1 (FTIR spectra of the synthesized SPIP are shown in Figure S1 in the SI), and therefore, it is an ideal system to probe the lithiation mechanism and the chemical structures involved in the reaction with lithium. Furthermore, the successful demonstration of the electrochemical activity of vulcanized

Received: April 18, 2016
Accepted: May 16, 2016

DOI: 10.1021/acsenergylett.6b00073
ACS Energy Lett. 2016, 1, 115−120

Scheme 1. Vulcanization of PIP

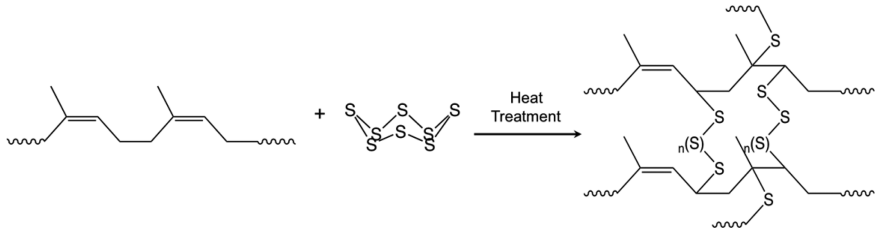

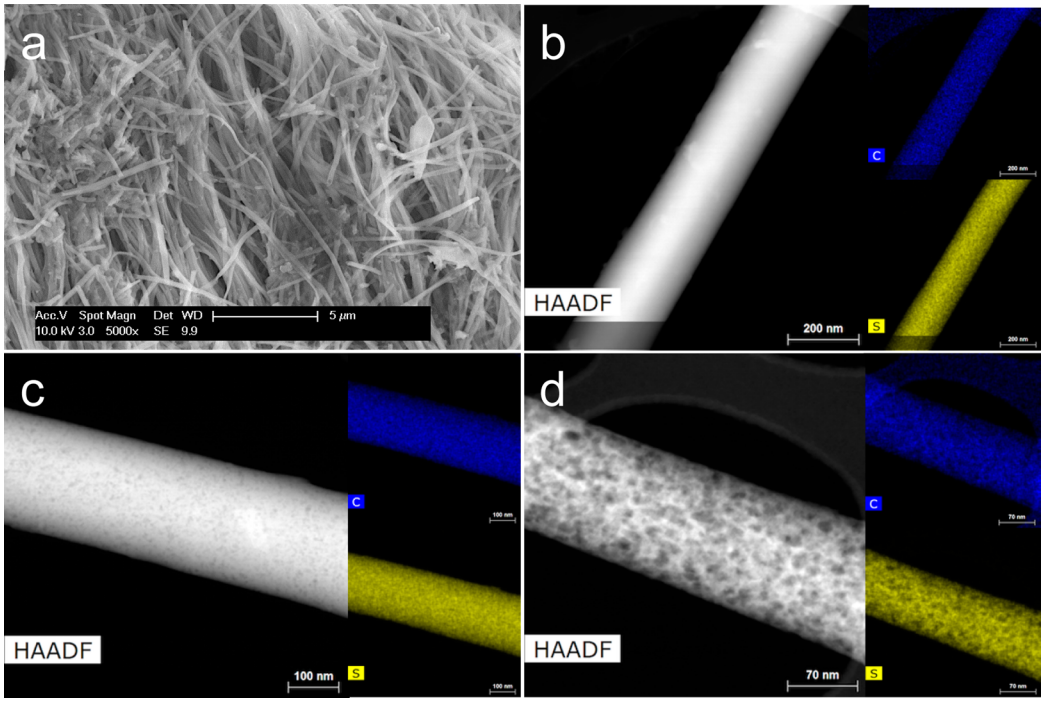

Figure 1. (a) SEM image of representative SPIP nanowires; HAADF-STEM images and elemental mappings of carbon and sulfur of (b) SPIP-250, (c) SPIP-300, and (d) SPIP-350 nanowires.

natural rubber toward Li can potentially lead to a highly economical, new renewable energy storage technology.

In this study, we synthesized SPIP following the classic process of natural rubber vulcanization shown in Scheme 1. SPIP was synthesized by uniformly mixing elemental sulfur and PIP followed by heat treatment in an argon environment at various temperatures including 250 °C (SPIP-250), 300 °C (SPIP-300), and 350 °C (SPIP-350). To achieve nanostructured SPIP to facilitate the Li ion transport, we templated the vulcanization reaction by using an anodic aluminum oxide (AAO) membrane, thereby allowing the synthesis of SPIP nanowires with a diameter of approximately 200 nm (see the Experimental Methods for details). Figure 1 shows a representative scanning electron microscopic (SEM) image and high-angle annular dark field scanning transmission electron microscopic (HAADF-STEM) images of the SPIP nanowires.

The SEM image clearly shows the macroscopic structure of the SPIP nanowires. It is also clear from the STEM images that different vulcanization temperatures induced different microscopic structures; SPIP-250 from the lowest temperature apparently has a smooth surface, indicating a relatively dense structure. The porosity of SPIP increases with vulcanization temperature as indicated by the unambiguous porous surface of SPIP-300 and SPIP-350. Nevertheless, the elemental mappings suggest uniform dispersion of sulfur throughout the organosulfur compounds in all samples. Powder X-ray diffraction (XRD Figure S2 in the SI) data indicate that all three SPIP compounds are amorphous. Sulfur elemental analysis via colorimetric titration shows that the sulfur contents in SPIP-250, SPIP-300, and SPIP-350 are 49.1, 48.2, and 25.4 wt %, respectively (Table S1 in the SI). We believe that the lower sulfur content in SPIP-350 is due to the high vulcanization temperature, which promoted PIP backbone decomposition and sulfur evaporation. It is consistent with the observation that SPIP-350 has the most porous structure among the three.

The cyclic voltammetry (CV) curves of the three SPIP compounds in Figure 2a all demonstrated distinctly different electrochemical behaviors from those of the typical unbonded elemental sulfur. SPIP-250 demonstrated four broad cathodic peaks from 2.6 to 1.75 V. The broad CV peaks indicate that the lithiation of sulfur chains in SPIP may be controlled by mass transport due to the tightly cross-linked molecular structure. The distinguishable multistep charge transfer process also indicates that lithiation of sulfur chains in SPIP undergoes a multistep charge transfer process following different lithiation mechanism from bulk sulfur and organosulfur polymers from inverse vulcanization. The anodic scan of SPIP-250 resulted to one prominent peak at 2.45 V and one broadened small peak at 3.0 V. The 2.45 V peak is believed to represent the delithiation

DOI: 10.1021/acsenergylett.6b00073
ACS Energy Lett. 2016, 1, 115−120

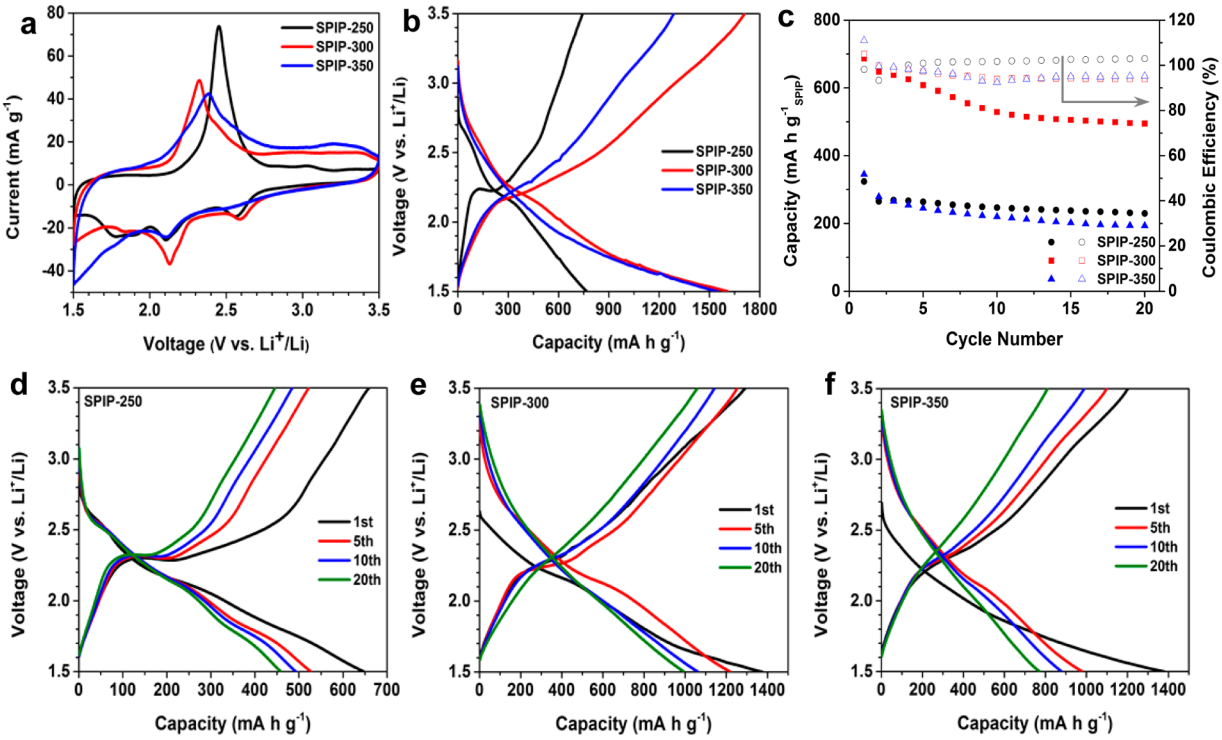

Figure 2. (a) CV scans with 0.05 mV s^{-1}, (b) galvanostatic lithiation−delithiation potential profiles at 10 mA g^{-1}, and (c) galvanostatic cycling stability at 50 mA g^{-1} of SPIP-250, SPIP-300, and SPIP-350. Galvanostatic cycling curves at various cycles of (d) SPIP-250, (e) SPIP-300, and (f) SPIP-350.

of the products generated from the anodic process at 2.1, 1.9, and 1.7 V. The 3.0 V anodic peak should be the reverse process of the high-potential lithiation at 2.6 V. It is worth noting that the potentials of this redox pair are significantly higher than any lithiation−delithiation potential of bulk sulfur. Therefore, it clearly indicates a new lithiation mechanism of the covalently bonded sulfur in SPIP. We speculate that this redox pair (2.6 V anodic vs 3.0 V cathodic) corresponds to the generation and delithiation of the −C−S−Li groups tethered on the PIP backbone. The CV curve of SPIP-300 is consistent with that of SPIP-250 except that it shows additional lithiation reactivity (i.e., broad cathodic peaks) below 2.0 V versus Li/Li^+. It becomes more distinct in the galvanostatic lithiation−delithiation potential profiles in Figure 2b (capacity based on the mass of sulfur) that the lithiation of SPIP-300 and SPIP-350 shows a slope profile below 2.0 V, which is responsible for the extra capacity compared to that of SPIP-250. The slope potential profile of SPIP-300 and SPIP-350 below 2.0 V is similar to the one we recently observed in a solid-state Li−S reaction not involving lithium polysulfides.[18] Therefore, we speculate that the low-potential lithiation in SPIP-300 as well as SPIP-350 is the lithiation of short sulfur chains (resulting from the higher vulcanization temperatures) directly resulting in nonsoluble lithium sulfide (Li_2S) and lithium disulfide (Li_2S_2) or low-solubility low-order polysulfides. This hypothesis is consistent with the previous finding by Wei and co-workers with S-PAN materials.[9] On the other hand, the lithiation mechanism of SPIP compounds seems to have some difference from that of S-PAN indicated by the multistep charge transfer process (i.e., multiple CV redox pairs at different potentials). It is also worth noting that unlike S-PAN, SPIP compounds show very different electrochemical characteristics in carbonate-based electrolyte (Figure S3 in the SI). Additional CV cycles and parallel comparison of CV and potential profiles of SPIP compounds are provided in the SI. As the cycle stability demonstrates in Figure 2c (specific capacity based on the mass of SPIP), both SPIP-300 and SPIP-350 show high specific capacity based on sulfur. The specific capacity of SPIP-250 is modest, although the capacity retention is stable. Figure 2d−f shows the lithiation−delithiation curves at various cycles of all three SPIP compounds. The difference in the potential profile from the initial cycle to the later ones, particularly for SPIP-300 and SPIP-350, indicates that all three SPIP compounds essentially follow the same electrochemical mechanism during the prolonged cycling.

To shed some light on the lithiation mechanism of the sulfur chains in SPIP, we performed X-ray photoelectron spectroscopy (XPS) on both pristine and lithiated SPIP samples. To prevent contamination, the lithiated samples were prepared in an argon-filled glovebox, and the XPS samples were inserted into the vacuum chamber via a load lock within a glovebox. The oxidized surface (solid electrolyte interface) was removed by ion beam etching. As shown in Figure 3, the XPS data of the SPIP samples are internally consistent; the S 2p spectra of the pristine samples mainly show elemental sulfur peaks at 164.0 eV (S $2p_{1/2}$) and 165.2 eV (S $2p_{3/2}$) (in orange). The peaks with higher binding energy than 167 eV are due to the sulfur oxide species from vulcanization.[19−21] The peaks at 162. 0 and 163.2 eV (in blue) represent the sulfur in a S−C single bond.[4] The C 1s spectra of the pristine SPIP samples show the typical C sp^2 peak at 284.5 eV (in blue) and the C sp^3 peak at 285.5 eV (in green). The peak at 286.0 eV (in orange) represents C−S single bonds.[4] After lithiation, the S 2p spectra show the typical lithiated sulfur peaks including Li_2S (161.0 and 162.2 eV in blue) and Li_2S_2 (162.0 and 163.2 eV in green).[18] It is worth noting that the binding energy of S in −C−S−Li is very similar

DOI: 10.1021/acsenergylett.6b00073
ACS Energy Lett. 2016, 1, 115−120

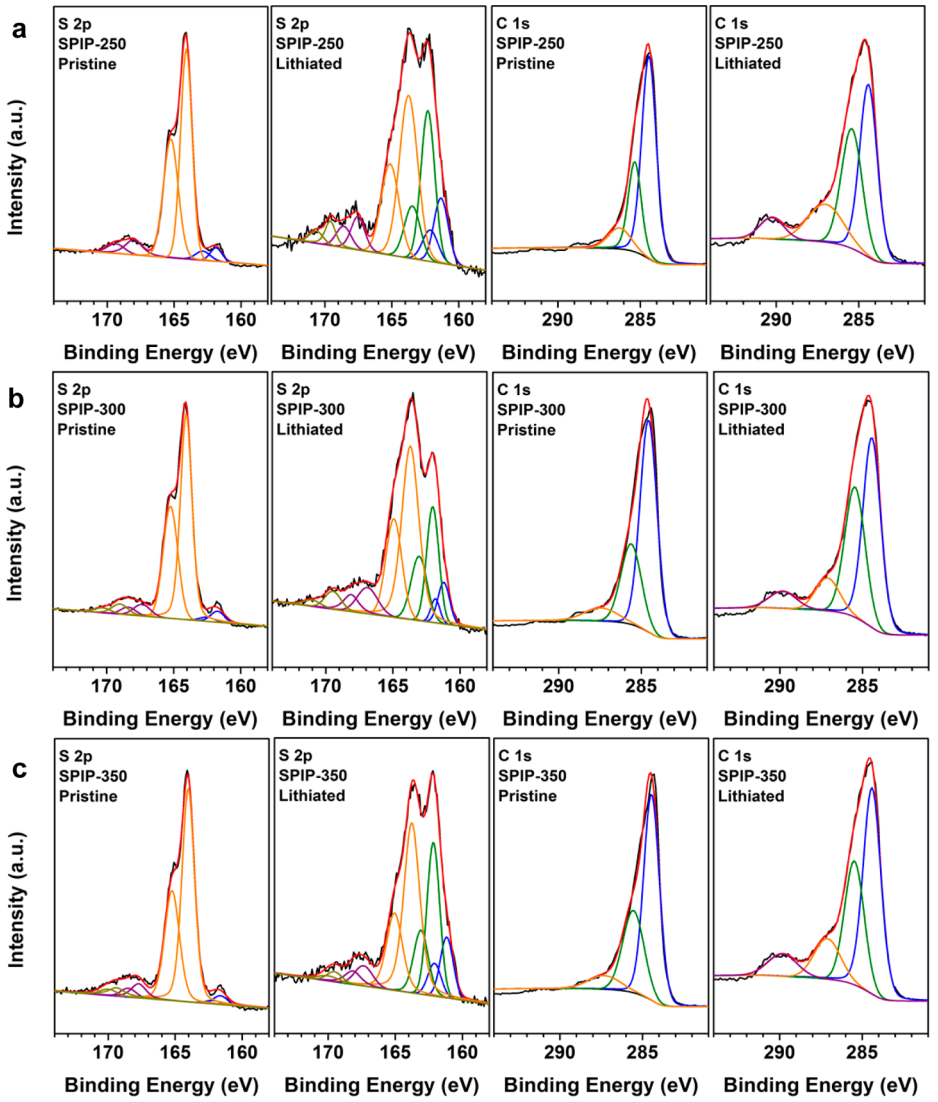

Figure 3. XPS spectra of S 2p and C 1s of the pristine and lithiated (a) SPIP-250, (b) SPIP-300, and (c) SPIP-350 compounds.

to the binding energy of S in Li_2S; thus, their XPS spectra may be superimposed. The C 1s spectra of the lithiated SPIP clearly show a new peak at 290.0 eV that can be assigned to the C═S thiocarbonyl group,[22] which apparently is formed during lithiation. It is also worth noting that the C−Li peak at 283.0 eV was not observed,[23] which indicates that the C−S linkage is intact during lithiation. Therefore, we suggest that the lithiation of sulfur chains in SPIP results in cleavage of the sulfur chains between the first and the second sulfur atom to form the −C−S−Li groups or C═S groups attached to the PIP backbone and untethered lithium sulfide species. This hypothesis is supported by the unconventional high-potential redox pair demonstrated in CV scans in Figure 2a.

The Raman spectra of the pristine SPIP compounds and the lithiated compounds at the 1st and the 10th cycles are shown in Figure 4. The pristine SPIP compounds show D and G modes at 1350 and 1480 cm^{-1} wavenumbers, respectively. The small peak at 498 cm^{-1} is attributed to the S−S deformation.[4] The peak at 834 cm^{-1} is due to C−S bond stretching,[24] although the C−S signal in SPIP-250 is relatively weak. After lithiation, a new peak appears at 564 cm^{-1}, which can be assigned to lithium sulfide species. Another new peak appears at 1100 cm^{-1}, which can be assigned to thiocarbonyl (C═S) bonds.[25] Meanwhile, the C−S peak seems to shift to an 800 cm^{-1} wavelength. As shown by the Raman spectra of the lithiated SPIP compounds at the 10th cycle, there is no significant difference between the 1st cycle and the 10th cycle. The only noticeable change is that the intensity of the C═S peak (1100 cm^{-1}) in SPIP-300 and SPIP-350 becomes higher. It is interesting that there is no noticeable change of the Raman spectra for SPIP-250, which also has the most stable cycle stability despite the modest capacity.

On the basis of the chemical changes apparent in the XPS and Raman spectroscopy studies, we propose the mechanisms of sulfur chain lithiation shown in Scheme 2. In the first possible pathway (a), the lithiation of sulfur chains results in −C−S−Li groups tethered on the PIP backbone and untethered lithium sulfide species subject to further lithiation. Pathway (a) is electrochemically reversible for delithiation; however, its reversibility (i.e., reconnecting the sulfur bridge) may be sterically hindered due to the redistribution of unbonded lithium sulfide species. In lithiation pathway (b), lithiation of sulfur chains in the presence of a sulfur free radical results in hydrogen abstraction and the formation of thiocarbonyl groups. Pathway (b) is not electrochemically reversible (i.e., the sulfur chains cannot be reconnected to the

DOI: 10.1021/acsenergylett.6b00073
ACS Energy Lett. 2016, 1, 115−120

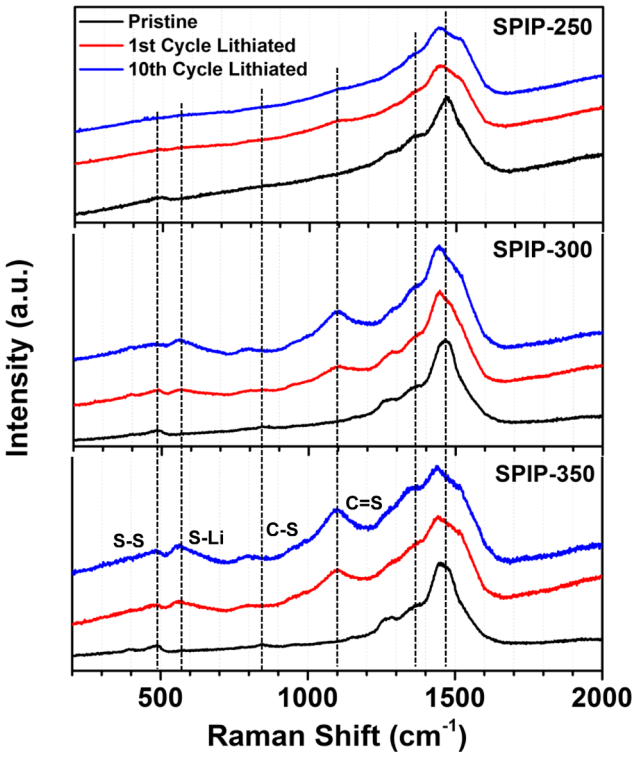

Figure 4. Raman spectra of the pristine and lithiated SPIP-250, SPIP-300, and SPIP-350 compounds.

C═S groups), although C═S may be active toward lithiation in subsequent cycling. The increased C═S signal intensity in Raman spectra with cycling (1st vs 10th) strongly indicates that the decay of cycle stability is mainly due to losing active sulfur to the formation of C═S groups. On the basis of these two proposed mechanisms, we believe that prolonged cycling will lead to the presence of noncovalently bonded sulfur molecules or clusters physically embedded in the PIP matrix, which explains the evolution of the potential profiles as a function of cycle number observed in Figure 2d–f.

In summary, the electrochemical lithiation of covalently bonded sulfur chains in vulcanized PIP demonstrates clearly distinct behavior from that of isolated elemental sulfur molecules and macromolecules, and these differences originate from the covalent bonding of sulfur species to the polymer backbone. Depending on the chain length, Li_2S, Li_2S_2, and lower-order polysulfides may be directly generated from lithiation-induced cleavage of the sulfur–sulfur bonds between the first and second atoms in the chain. Both reversible and irreversible lithiation processes are available; however, the practical reversibility may be determined by the redistribution of the untethered lithium sulfide species and the steric effects from the cross-linked network. The undesirable capacity decay of the SPIP compounds may be due to the formation of irreversible C═S groups and possible thiol species during electrochemical lithiation. The SPIP compounds also show limited rate capability due to the low electrical conductivity. Nevertheless, vulcanized PIP represents a new prototype cathode material for rechargeable lithium batteries, and we expect that chemically modified variants in which the sulfur chains are bonded to polymeric backbones with branching side groups and heteroatoms may further improve the electrochemical characteristics of this class of materials.

EXPERIMENTAL METHODS

Synthesis of SPIP Nanowires. In a typical synthesis, 0.75 g of *cis*-1,4-PIP (Sigma-Aldrich) and 2.75 g of sulfur (Sigma-Aldrich) were first codissolved in 10 mL of carbon disulfide (CS_2, Alfa Aesar) in a 20 mL autoclave with AAO templates (Whatman) immersed in the solution. The autoclave was heated at 155 °C for 15 h to yield a dark brown gel. The AAO templates were then taken out of the gel and dried at 70 °C for 5 h, followed by heating at 250, 300, or 350 °C for 10 h in a sealed tube filled with argon. The AAO template was dissolved by washing with 1 M NaOH solution. The resulting SPIP compounds were collected by filtration and dried at 70 °C for 5 h; the free sulfur was removed by thoroughly rinsing with CS_2.

Materials Characterizations. The crystallinity of the SPIP compounds was characterized with X-ray powder diffraction (PANalytical Empyrean). Fourier transform infrared spectroscopy (FTIR, Nicolet 6700) and Raman spectroscopy (Nicolet Almega XR with 532 nm wavelength laser source) were used to characterize the chemical structure of the compounds. The chemical state of sulfur and carbon in the SPIP compound was characterized with X-ray photoelectron spectroscopy (XPS, AXIS Supra). Transmission electron microscopy (STEM FEI Titan 300) coupled with an energy dispersive X-ray (EDX) spectrometer was used to obtain the HAADF-STEM images and the elemental mappings of the compounds. SEM images were taken with a FEI XL30-FEG.

Electrochemical Analysis. The electrodes were comprised of 70 wt % SPIP compound, 20 wt % carbon black (Super P), and 10 wt % PVP (Sigma-Aldrich) binder. The areal loading of SPIP compound in the electrode was approximately 2.5 ± 0.2 mg cm^{-2}. Aluminum foil (99.45%, Alfa Aesar) was used as the

Scheme 2. Proposed Lithiation Mechanisms: (a) Reversible Pathway Leading to −C−S−Li and Lithium Sulfide Species and (b) Irreversible Pathway Leading to −C═S and Lithium Sulfide Species

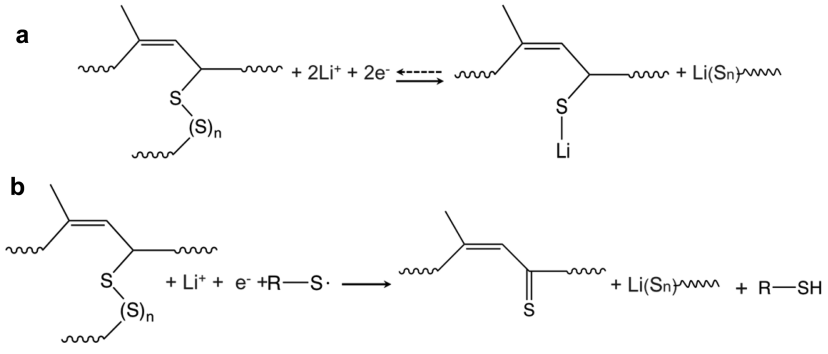

DOI: 10.1021/acsenergylett.6b00073
ACS Energy Lett. 2016, 1, 115–120

current collector. Two-electrode coin cells with lithium foil (Alfa Aesar) as the counter electrode were assembled in an argon-filled glovebox for the electrochemistry analysis. The electrolyte consisted of 1 M lithium hexafluorophosphate ($LiPF_6$, Sigma-Aldrich) in tetraglyme (Sigma-Aldrich) used in conjunction with a microporous membrane separator (Celgard 2500). The cells were discharged and charged with various cycling currents between 1.5 and 3.5 V (vs Li^+/Li) using an Arbin battery test station. CV scans were carried out with a scan rate of 0.05 mV s^{-1} on a Gamry Interface 1000 analyzer. All of the electrochemical analyses were performed at room temperature.

■ ASSOCIATED CONTENT

Supporting Information

The Supporting Information is available free of charge on the ACS Publications website at DOI: 10.1021/acsenergylett.6b00073.

Schematic synthesis process, FTIR spectra, XRD patterns, sulfur analysis, electrochemical characterization in carbonate-based electrolyte, additional CV scans of SPIP compounds, and parallel comparison of CV scans and charge−discharge potential profiles (PDF)

■ AUTHOR INFORMATION

Corresponding Author

*E-mail: jguo@engr.ucr.edu.

Notes

The authors declare no competing financial interest.

■ ACKNOWLEDGMENTS

This material is based upon work supported by Power Energy Solutions Inc.

■ REFERENCES

(1) Naoi, K.; Kawase, K.; Inoue, Y. A new energy storage material: organosulfur compounds based on multiple sulfur-sulfur bonds. *J. Electrochem. Soc.* **1997**, *144*, L170−L172.

(2) Bresser, D.; Passerini, S.; Scrosati, B. Recent progress and remaining challenges in sulfur-based lithium secondary batteries - a review. *Chem. Commun.* **2013**, *49*, 10545−10562.

(3) Wang, J.; Yang, J.; Wan, C.; Du, K.; Xie, J.; Xu, N. Sulfur composite cathode materials for rechargeable lithium batteries. *Adv. Funct. Mater.* **2003**, *13*, 487−492.

(4) Yu, X. G.; Xie, J. Y.; Yang, J.; Huang, H. J.; Wang, K.; Wen, Z. S. Lithium storage in conductive sulfur-containing polymers. *J. Electroanal. Chem. Interfacial Electrochem.* **2004**, *573*, 121−128.

(5) Yin, L.; Wang, J.; Yang, J.; Nuli, Y. A novel pyrolyzed polyacrylonitrile sulfur@MWCNT composite cathode material for high-rate rechargeable lithium/sulfur batteries. *J. Mater. Chem.* **2011**, *21*, 6807−6810.

(6) Yin, L.; Wang, J.; Lin, F.; Yang, J.; Nuli, Y. Polyacrylonitrile/graphene composite as a precursor to a sulfur-based cathode material for high-rate rechargeable Li−S batteries. *Energy Environ. Sci.* **2012**, *5*, 6966−6972.

(7) Fanous, J.; Wegner, M.; Grimminger, J.; Andresen, Ä.; Buchmeiser, M. R. Structure-related electrochemistry of sulfur-poly(acrylonitrile) composite cathode materials for rechargeable lithium batteries. *Chem. Mater.* **2011**, *23*, 5024−5028.

(8) Zhang, S. S. Understanding of sulfurized polyacrylonitrile for superior performance lithium/sulfur battery. *Energies* **2014**, *7*, 4588−4600.

(9) Wei, S.; Ma, L.; Hendrickson, K. E.; Tu, Z.; Archer, L. A. Metal-sulfur battery cathodes based on PAN-sulfur composites. *J. Am. Chem. Soc.* **2015**, *137*, 12143−12152.

(10) Chung, W. J.; Griebel, J. J.; Kim, E. T.; Yoon, H.; Simmonds, A. G.; Ji, H. J.; Dirlam, P. T.; Glass, R. S.; Wie, J. J.; Nguyen, N. A.; et al. The use of elemental sulfur as an alternative feedstock for polymeric materials. *Nat. Chem.* **2013**, *5*, 518−524.

(11) Simmonds, A. G.; Griebel, J. J.; Park, J.; Kim, K. R.; Chung, W. J.; Oleshko, V. P.; Kim, J.; Kim, E. T.; Glass, R. S.; Soles, C. L.; et al. Inverse vulcanization of elemental sulfur to prepare polymeric electrode material for Li-S batteries. *ACS Macro Lett.* **2014**, *3*, 229−232.

(12) Griebel, J. J.; Li, G.; Glass, R. S.; Char, K.; Pyun, J. Kilogram scale inverse vulcanization of elemental sulfur to prepare high capacity polymer electrodes for Li-S batteries. *J. Polym. Sci., Part A: Polym. Chem.* **2015**, *53*, 173−177.

(13) Arslan, M.; Kiskan, B.; Yagci, Y. Combining elemental sulfur with polybenzoxazines via inverse vulcanization. *Macromolecules* **2016**, *49*, 767−773.

(14) Sun, Z.; Xiao, M.; Wang, S.; Han, D.; Song, S.; Chen, G.; Meng, Y. Sulfur-rich polymeric materials with semi-interpenetrating network structure as a novel lithium-sulfur cathode. *J. Mater. Chem. A* **2014**, *2*, 9280−9286.

(15) Dirlam, P. T.; Simmonds, A. G.; Kleine, T. S.; Nguyen, N. A.; Anderson, L. E.; Klever, A. O.; Florian, A.; Costanzo, P. J.; Theato, P.; Mackay, M. E.; et al. Inverse vulcanization of elemental sulfur with 1,4-diphenylbutadiyne for cathode materials in Li-S batteries. *RSC Adv.* **2015**, *5*, 24718−24722.

(16) Kim, H.; Lee, J.; Ahn, H.; Kim, O.; Park, M. J. Synthesis of three-dimensionally interconnected sulfur-rich polymers for cathode materials of high-rate lithium-sulfur batteries. *Nat. Commun.* **2015**, *6*, 7278.

(17) Talapaneni, S. N.; Hwang, T. H.; Je, S. H.; Buyukcakir, O.; Choi, J. W.; Coskun, A. Elemental-sulfur-mediated facile synthesis of a covalent triazine framework for high-performance lithium-sulfur batteries. *Angew. Chem., Int. Ed.* **2016**, *55*, 3106−3111.

(18) Fu, C.; Wong, B. M.; Bozhilov, K. N.; Guo, J. Solid state lithiation-delithiation of sulphur in sub-nano confinement: a new concept for designing lithium-sulphur batteries. *Chem. Sci.* **2016**, *7*, 1224−1232.

(19) Fu, Y.; Zu, C.; Manthiram, A. In situ-formed Li_2S in lithiated graphite electrodes for lithium-sulfur batteries. *J. Am. Chem. Soc.* **2013**, *135*, 18044−18047.

(20) Su, Y.-S.; Fu, Y.; Cochell, T.; Manthiram, A. A strategic approach to recharge Li-S batteries for long cycle life. *Nat. Commun.* **2013**, *4*, 2985.

(21) Tao, X.; Wang, J.; Ying, Z.; Cai, Q.; Zheng, G.; Gan, Y.; Huang, H.; Xia, Y.; Liang, C.; Zhang, W.; et al. Strong sulfur binding with conducting Magnéli-phase Ti_nO_{2n-1} nanomaterials for improving lithium−sulfur batteries. *Nano Lett.* **2014**, *14*, 5288−5294.

(22) Moulder, J. F.; Stickle, W. F.; Sobol, P. E.; Bomben, K. D. In *Handbook of X-ray Photoelectron Spectroscopy*; Chastain, J., King, R. C., Eds.; Physical Electronics USA, Inc.: Chanhassen, MN, 1995; pp 41.

(23) Zu, C.; Manthiram, A. High-performance Li/dissolved polysulfide batteries with an advanced cathode structure and high sulfur content. *Adv. Energy Mater.* **2014**, *4*, 1400897.

(24) Bloxham, S.; Eicher-Lorka, O.; Jakubėnas, R.; Niaura, G. The C-S bond in ethyl thiols: a study of the characteristic Raman vibrational spectral band. *Chemija* **2002**, *13*, 190−193.

(25) Cao, P.; Yao, J.; Ren, B.; Gu, R.; Tian, Z. Surface-enhanced Raman scattering spectra of Thiourea adsorbed at an iron electrode in $NaClO_4$ solution. *J. Phys. Chem. B* **2002**, *106*, 10150−10156.

DOI: 10.1021/acsenergylett.6b00073
ACS Energy Lett. 2016, 1, 115−120

Supporting Information

Electrochemical Lithiation of Covalently Bonded Sulfur in Vulcanized Polyisoprene

Chengyin Fu,[1] Guanghui Li,[1,2] Jian Zhang,[1] Benjamin Cornejo,[1] Sophie S. Piao,[3] Krassimir N. Bozhilov,[4] Robert C. Haddon,[1,2,5] Juchen Guo[1]*

[1]Department of Chemical and Environmental Engineering, University of California, Riverside, California 92521, United States

[2]Center for Nanoscale Science and Engineering, University of California, Riverside, California 92521, United States

[3]Division of Chemistry and Chemical Engineering, California Institute of Technology, Pasadena, California 91125, United States

[4]Central Facility for Advanced Microscopy and Microanalysis, University of California, Riverside, CA 92521, United States

[5]Department of Chemistry, University of California, Riverside, California 92521, United States

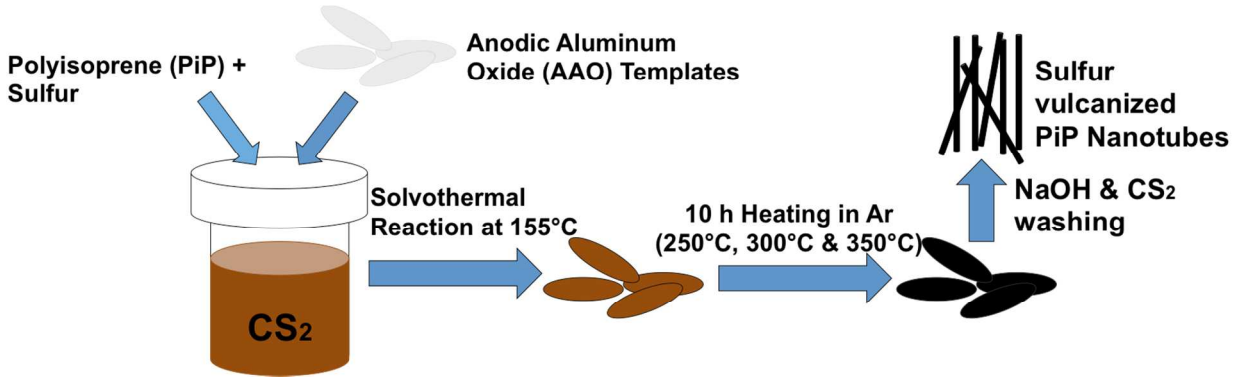

Scheme S1. Synthetic process of SPIP nanowires.

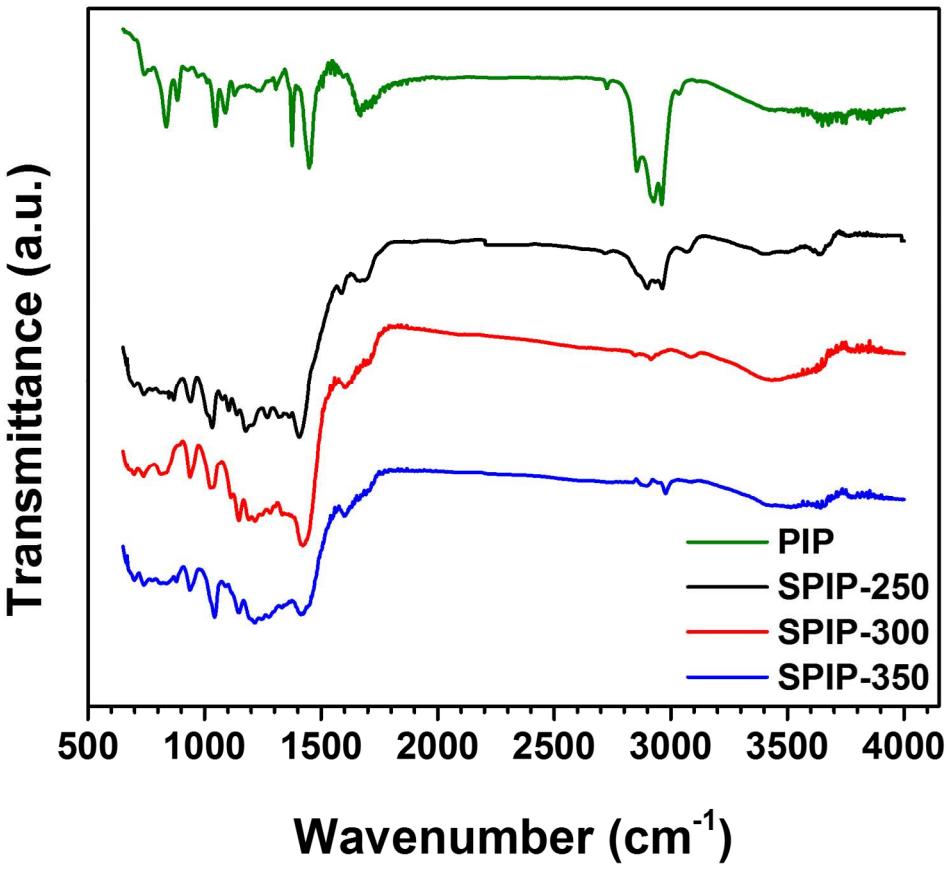

Figure S1. FTIR spectra of the pristine PIP, vulcanized SPIP-250, SPIP-300 and SPIP-350. The spectra of pristine PIP clearly show the C=C stretch at 1680 cm^{-1}, C-H and =C-H_2 stretches between 2850 cm^{-1} to 3050 cm^{-1}. The magnitudes of all these peaks are reduced after vulcanization but remain detectable, indicating vulcanization reactions including free radical addition to the vinyl group and dehydrogenization of the allylic hydrogens.

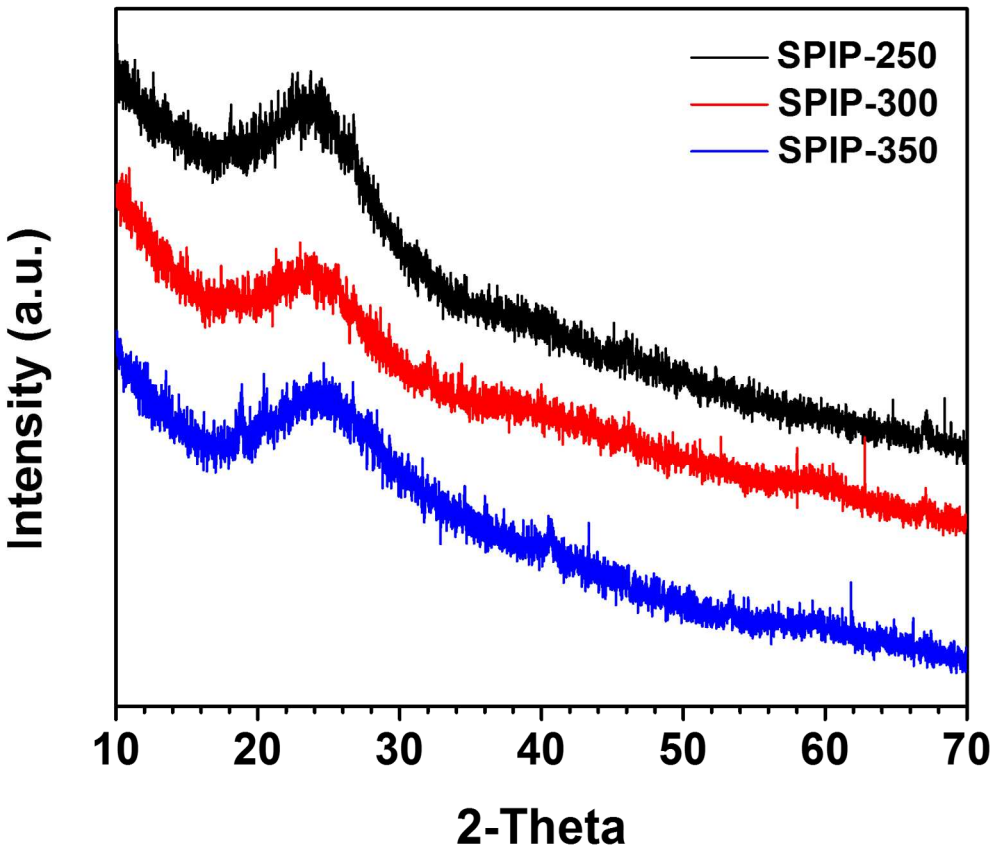

Figure S2. Powder XRD pattern of SPIP-250, SPIP-300 and SPIP-350 compounds.

EAI ~ Elemental Analysis, Inc.

Thursday, April 14, 2016

Dr. Juchen Guo,
University of California, Riverside
900 University Ave Bourns Hall A220
Riverside CA 92521

Phone: (951) 827-6472
Email: jguo@engr.ucr.edu

EAI Project: 2749-16

Sulfur by Colorimetric Titration

Sample ID	Sulfur (wt%)
SPIP 250°C	49.13%
SPIP 300°C	48.25%
SPIP 350°C	25.45%

Respectfully Submitted,
Elemental Analysis Incorporated

Nick Tzouanakis,
Technical Sales Representative

2101 Capstone Drive, Suite 110, Lexington, KY 40511
Phone: 800-563-7493 / Fax: 859-254-5150 Email: Trace@ElementalAnalysis.com

Table S1. Sulfur content analysis of SPIP-250, SPIP-300 and SPIP-350 performed by Elemental Analysis Incorporated.

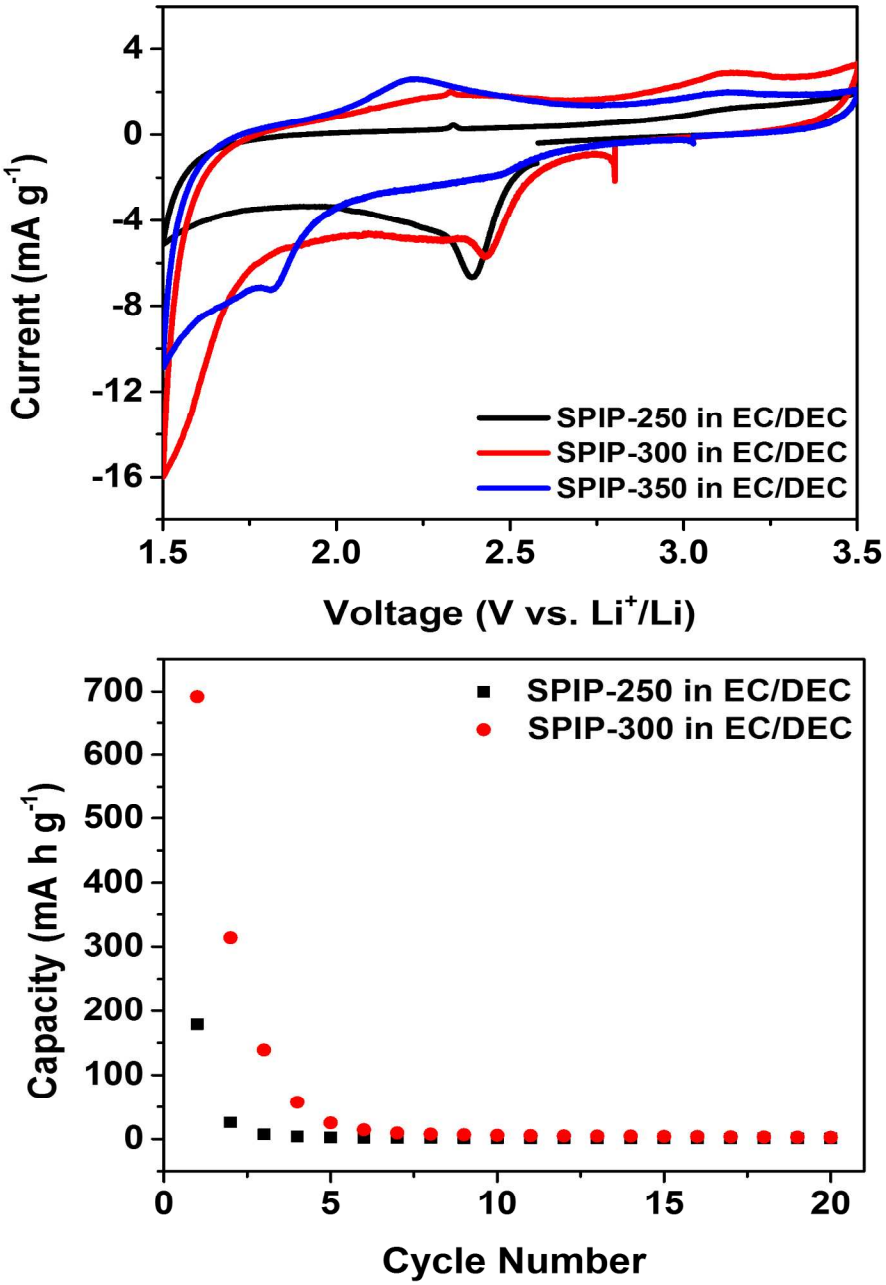

Figure S3. CV scans and cycle stability of SPIP compounds in electrolyte composed of 1 M $LiPF_6$ in ethylene carbonate/diethyl carbonate (50/50 volume ratio).

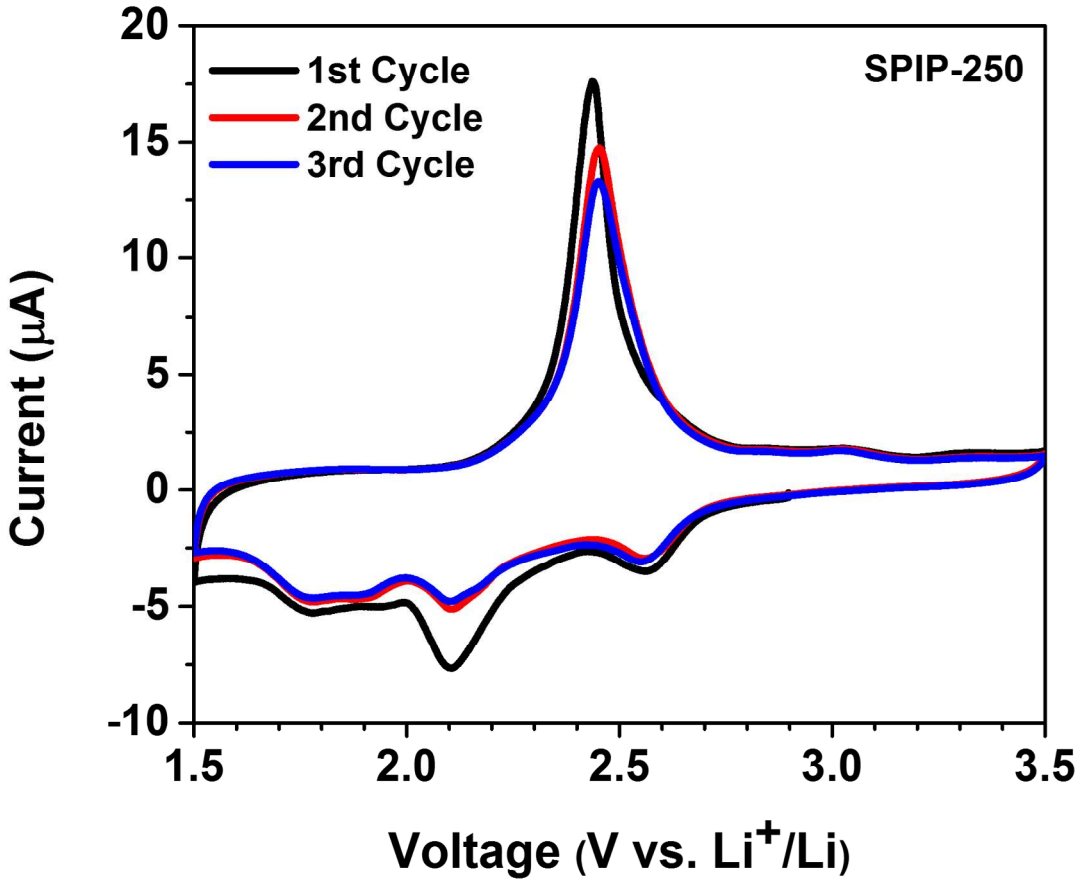

Figure S4. Complete three CV cycles of SPIP-250.

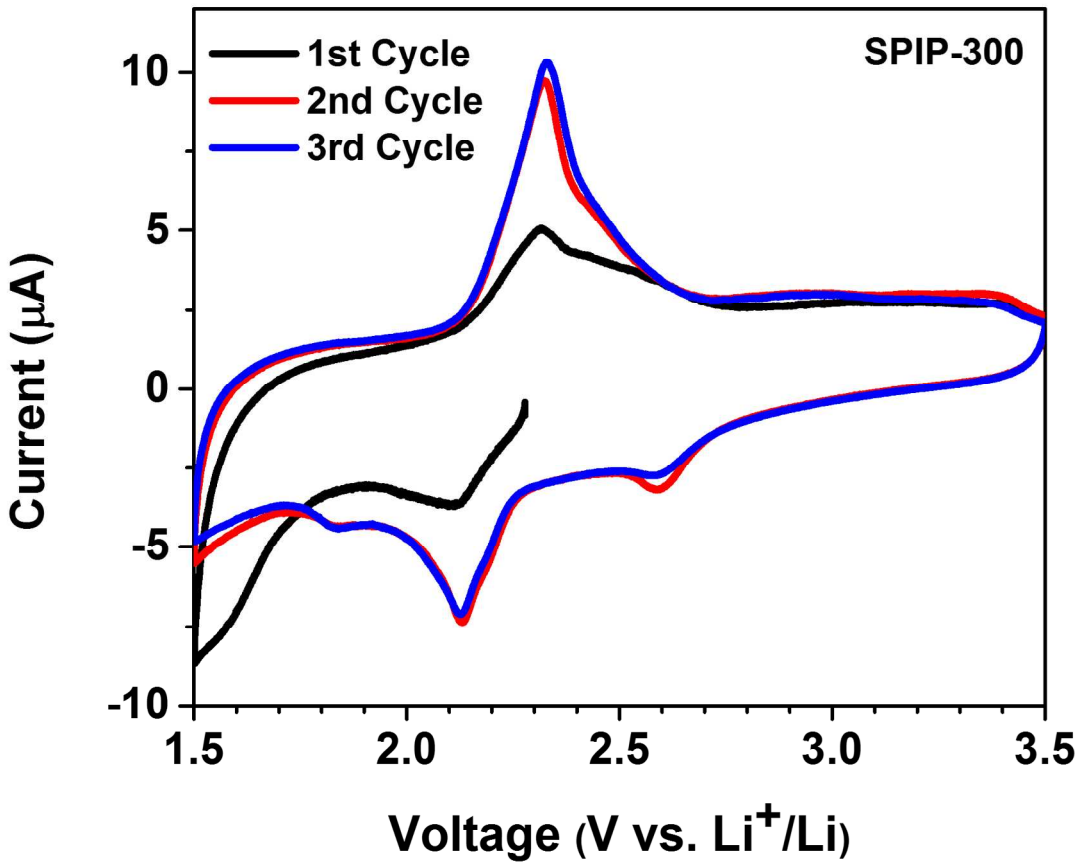

Figure S5. Complete three CV cycles of SPIP-300.

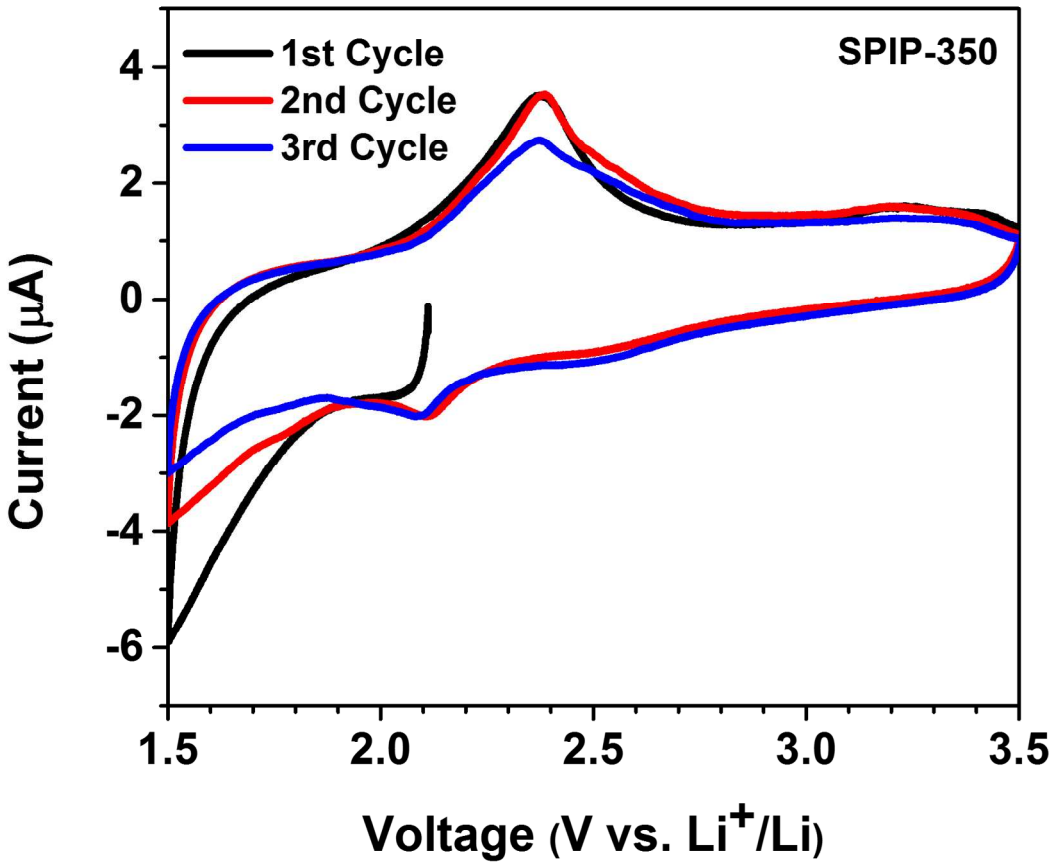

Figure S6. Complete three CV cycles of SPIP-350.

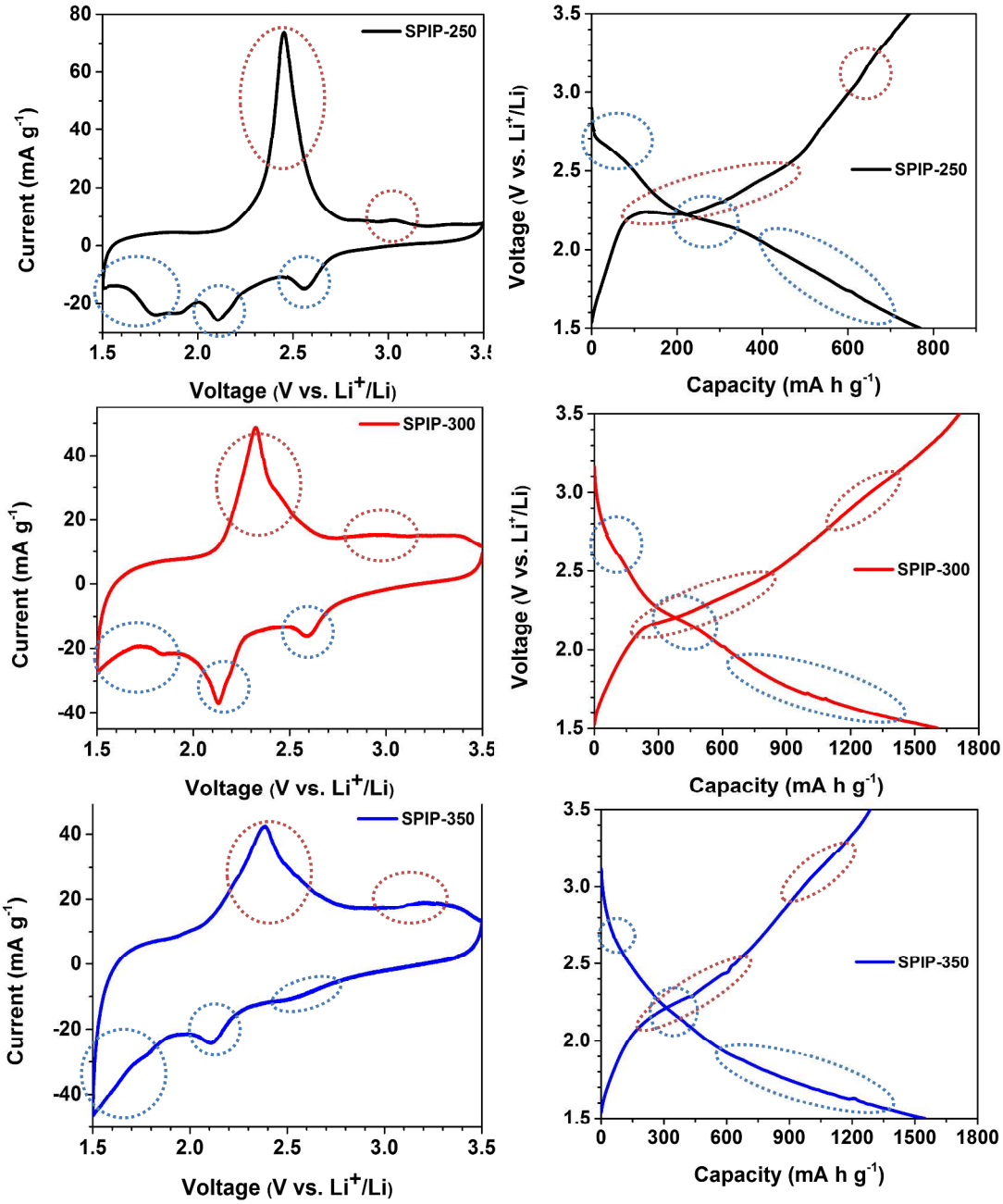

Figure S7. Parallel comparison of CV curves and charge-discharge potential profiles of each SPIP compound.